Pharm Res (2012) 29:158–169
DOI 10.1007/s11095-011-0522-6

RESEARCH PAPER

# Polymer-Mediated Anti-solvent Crystallization of Nitrendipine: Monodispersed Spherical Crystals and Growth Mechanism

Dengning Xia • Mei Ouyang • Jian X. Wu • Yanbo Jiang • Hongyu Piao • Shaoping Sun • Li Zheng • Jukka Rantanen • Fude Cui • Mingshi Yang

Received: 19 April 2011 / Accepted: 27 June 2011 / Published online: 12 July 2011
© Springer Science+Business Media, LLC 2011

## ABSTRACT

***Purpose*** To investigate anti-solvent crystallization and growth mechanism of nitrendipine spherical crystals in an aqueous solution containing polymeric additives.

***Methods*** Size and shape of crystals were investigated using laser diffractometry, optical microscopy and scanning electron microscopy (SEM). Crystalline form was determined by X-ray powder diffractometer (XRPD). During crystal growth, morphological changes at different time points were observed using SEM.

***Results*** Morphology of nitrendipine crystals was affected by polymers and temperature. Monodispersed micro-spherical crystals were obtained when polyvinyl alcohol (PVA) and PEG 200 were present in crystallization medium at 2°C. During crystallization, large number of amorphous nanoparticles was first observed, followed by aggregation into a core for spherical crystals. Once crystalline state was achieved, rapid growth on core surface was observed with amorphous particles acting as a reservoir allowing formation of star-like particles with needle-like subunits. Spherical crystals were formed by filling the gap between needle-like distinct crystalline units of star-like templates with molecules from dissolved amorphous particles.

***Conclusions*** Monodispersed nitrendipine spherical crystals were obtained using carefully controlled conditions. A mechanism for the nitrendipine spherical crystal growth is suggested. These findings provide a new insight into spherulitic crystallization of active pharmaceutical ingredients.

**KEY WORDS** amorphous · anti-solvent crystallization · crystal growth · nitrendipine · spherical crystals

## INTRODUCTION

Crystallization is central for many processes occurring in nature and in the chemical and pharmaceutical industries (1). The crystal morphology, particle size and particle size distribution of pharmaceutical ingredients are important, because they influence many of the crystal properties, such as the flowability, compressibility, and mixing homogeneity, and compounds with different crystal habits can also exhibit difference in dissolution rate (2,3), resulting in different oral bioavailability (4,5).

Anti-solvent crystallization is an effective way to prepare micro- or nano-size drug particles. In this method, the drug is first dissolved in a solvent to form a drug solution (organic phase), then the drug solution is quickly introduced into an anti-solvent. Precipitation occurs immediately by the rapid desolvation of the drug (6). Aqueous solutions (aqueous phase) containing some stabilizers, such as polymers and surfactants, are commonly used as the anti-solvent for drug in organic solution. Polymers, such as hydroxypropylmethylcellulose (HPMC) (7) and methylcellulose (MC) (8), and

D. Xia • M. Ouyang • Y. Jiang • H. Piao • S. Sun • L. Zheng • F. Cui (✉)
Department of Pharmaceutics, School of Pharmaceutical Science
Shenyang Pharmaceutical University
No. 103, Wenhua Road
Shenyang 110016, China
e-mail: dengningxia@qq.com

D. Xia • J. X. Wu • J. Rantanen • M. Yang
Department of Pharmaceutics and Analytical Chemistry
Faculty of Pharmaceutical Sciences, University of Copenhagen
Universitetsparken 2
2100 Copenhagen, Denmark

S. Sun
School of Chemistry and Material Science, Heilongjiang University
No. 74, Xuefu Street
Harbin 150080, China

polyvinylpyrrolidone (PVP) (9), can be adsorbed on the hydrophobic particle surface by hydrogen bonding (10), inhibiting the crystal growth of the drug and, thus, may influence the morphology of the crystals (11). Other external factors can also affect the crystal morphology, such as the temperature, solvent, and impurity concentration, which may cause an alteration in nucleation, the rate of deposition at any crystal surface, and even the mechanism of crystal growth involved (12,13). To be able to control and optimize the properties of crystals, it is essential to understand the growth mechanism of crystals, and it is necessary to take into account the effect of the process parameters on the crystallization involved in the anti-solvent crystallization system.

Monodispersed spherical crystals are often found in inorganic materials such as calcium carbonate (14,15), CdS (16), and ZnO (17), and in some organic polymers (18) and proteins (19), but there is much less information about small organic active pharmaceutical ingredients. It has been experimentally established in numerous cases that the precipitation of monodispersed crystals from homogeneous solutions is a complex process. An early mechanism (the classical crystallization process) of the formation of monodispersed crystals was based on the theory suggested by Reiss (20) and by LaMer and Dinegar (21), which assumes a short nucleation burst, followed by diffusional growth of the resulting nuclei *via* molecule-by-molecule addition to form identical fine crystals. Later, ample experimental evidence was obtained, demonstrating that some of those crystals were formed by a particle-mediated process, namely aggregation, self-assembly, and mesoscopic transformation of nanoparticles coupled via a restructuring process (17,22–24). In anti-solvent crystallization, particle formation takes place at the same time as mixing (25). The primary nanoparticles which are nucleated in a supersaturated solution are usually amorphous and metastable (26). Aggregation of those nanoparticles can produce amorphous, polycrystalline, or single crystals, depending on their structure, whether the aggregation process is random or directional and whether recrystallization occurs after aggregation (27–29). Although spherical crystals are easily recognizable under the optical microscope, there is as yet no unique description of their formation and growth. There is no generally accepted theory of spherulite crystallization, although a number of phenomenological models and the physical conditions required for this process have been suggested (18,30,31), and the kinetics leading to the final stable crystalline phase from metastable phases are so far poorly understood.

In the current study, the use of an anti-solvent crystallization method to produce micrometer-sized crystals was investigated. Spherical crystals with a uniform particle size distribution were obtained under carefully controlled conditions. During the crystal growth process, the morphological changes at different time points were observed, offering considerable insight into the mechanism of formation of nitrendipine spherical crystals. On the basis of these experimental results, a model for the formation of monodispersed spherical crystals during anti-solvent crystallization was formulated and discussed.

## MATERIALS AND METHODS

### Materials

Nitrendipine (as starting material) was purchased from Nanjing Pharmaceutical Factory (China). Lutrol®F127 (Poloxamer 407) was supplied by BASF Aktiengesellschaft (Germany). Metolose® (HPMC, grade 60SH-50, viscosity 50 cP) and polyvinyl alcohol (PVA, Mw 30-70 kDa, 88% alcoholysis) were generously supplied by Shin-Etsu Chemical Ind. Co. Ltd. (Japan). PEG 200 and acetone of analytical grade were purchased from Ruijingte Chemical Agent Company (Tianjing, China). All other chemicals were analytical grade.

### Crystalline Solubility Measurement and Theoretical Estimation of Amorphous Solubility Advantage

The solubility of nitrendipine in crystallization medium was measured. An excess of nitrendipine starting material was added to 10 ml mixed solvents of water and organic phase to form saturated solutions. After 48 h stirring, the samples were passed through a 0.22 μm filter (Xinya Purifier Device Factory, Shanghai, China). The drug concentration of the saturated solutions was determined by HPLC (Pump model: Hitachi L7110, Japan). The analytical column was a Diamonsil™ C18 (5 μm, 200×4.6 mm), the mobile phase was composed of methanol and water (75/25, v/v) at a flow rate of 1.0 ml/min, and the detection was performed at 236 nm using a UV-VIS detector (Model: Hitachi L7420, Japan).

As to the amorphous solubility advantage of nitrendipine, thermodynamically, the amorphous state is unstable relative to the crystalline state. It is difficult to obtain the solubility of the amorphous state using conventional methods, because the amorphous state is easily transformed into another more stable form. The solubility difference between the crystalline and amorphous phase is related to the chemical potential difference between the two states (32). The theoretical calculation method proposed by Brick *et al.* involves several reversible thermodynamic paths assuming that the amorphous state is equivalent to a supercooled liquid solution of the solute, and the relationship between the amorphous solubility, $C_{amorphous}$, and the

crystalline solubility, $C_{crystalline}$, is given by the following equation (33):

$$C_{amorphous} = C_{crystalline} \exp\left[\frac{\Delta H_M}{R_g T}\left(1 - \frac{T}{T_M}\right)\right] \quad (1)$$

where $R_g$ is the gas constant, and $T$ and $T_M$ are the absolute temperature and melting point of the crystals (K), respectively. The molar enthalpy of melting, $\Delta H_M$ and $T_M$ can be measured by differential scanning calorimetry (DSC).

## Rheology of the Crystallization Medium

The kinematic viscosity, $v$, ($m^2/s$) of crystallization medium was determined using a U-tube Viscometer (Pinkevitch type, Shenyang Huaqiao glass instrument factory, Shenyang) according to the method in the Chinese Pharmacopoeia (2005 Ed). Measurements were performed in a thermostatically controlled water bath, and the solutions were allowed to equilibrate at a preset temperature for 15 min before measuring the flow time. The flow time of each solution was measured in triplicate. The kinematic viscosity of the solution can be calculated from the Eq. 2, where $K$ is a constant for the apparatus, determined by measurements using pure water of known viscosity:

$$v = Kt \quad (2)$$

The kinematic viscosity can be converted to the dynamic viscosity, $\eta$, (Pa·s) according to Eq. 3:

$$\eta = v \times \rho \quad (3)$$

where $\rho$ is the density of the solutions in $kg/m^3$, and these values were obtained by measuring the solution mass and volume.

## Anti-solvent Crystallization of Nitrendipine

Nitrendipine was dissolved in mixed solvents of PEG 200 and acetone (percentage volume of PEG 200 varied from 0% to 100%, v/v) to form a series of drug organic solutions containing 15–100 mg/ml of drug. Aqueous solutions containing different types of stabilizers (PVA, HPMC and Poloxamer 407) with different concentrations (0.1%–2.0%, w/v) were thermostatically controlled (2, 15, 35°C) in a water bath (SDC-6, Ningbo Scientz Biotechnology Co. Ltd., China). All solutions were passed through 0.22 μm filler (Xinya Purifier Device Factory, Shanghai, China) to remove visible particles. To precipitate the drug, 2 ml of the organic phase containing the drug was added quickly by syringe to 20 ml of aqueous solution under magnetic stirring at approximately 400 rpm. The samples were kept at the same temperature for several hours to make sure that a stable crystal size was obtained. Each crystallization experiment was repeated three times.

## Characterization of Crystals

### Crystal Size Determination

The particle size of the initial particles (the particle size was determined within 30 s after the organic phase was mixed with the aqueous phase) and final crystals were determined by laser diffractometry using a Coulter LS230 instrument (Beckman-Coulter Co. Ltd., USA) combining laser diffraction and polarization intensity differential scattering (PIDS) method. Particle size and size distribution were created by the Beckman Coulter LS software (Version 3.19, Beckman Coulter, Inc., USA). The average particle size is expressed as the volume-mean diameter. The particle size distributions were evaluated by span, defined as

$$span = \frac{D90 - D10}{D50} \quad (4)$$

where D10, D50, D90 correspond to the diameters at which the cumulative volume was under 10%, 50% and 90%, respectively.

### Crystal Morphology

The crystal morphology was investigated by scanning electron microscopy (SEM, S-3400 instrument, Hitachi, Japan). The samples were dried and coated with gold for conductivity, and the accelerating voltage of 20 kV was used. The shape of final crystals in suspension was also observed using optical microscopy (Motic DMBA450 microscope, China) and transmitted polarized light microscopy (Axiolab, Carl Zeiss, Göttingen, Germany).

### X-ray Powder Diffraction (XRPD) Characterization

X-ray powder diffractograms were determined using a PANalytical X'Pert Pro diffractometer equipped with a PIXcel detector (PANalytical B.V., Almelo, the Netherlands). Samples were placed on zero-background silicon plates and measured at ambient conditions in reflection mode. A continuous $2\theta$ scan was performed in the range 5°–45° with a step size of 0.026° using Cu Kα radiation (λ = 1.5418Å). The voltage and current applied were 40 mA and 45 kV, respectively. The scanning speed was 0.5252° $2\theta$/s. Data were collected using X'Pert Data Collector software and processed using X'Pert HighScore Plus (PANalytical B.V.). The XRPD patterns of nitrendipine were verified by comparing the experimental XRPD patterns with the theoretical diffractogram obtained from

the Cambridge Crystallographic Data Centre (CCDC) using Mercury 2.4 (CCDC, Cambridge, UK). A reference code JEXKUS was used to generate the theoretical diffraction patterns of crystalline nitrendipine.

### *Differential Scanning Calorimetry (DSC) Characterization*

The melting point, $T_M$, and enthalpy of melting, $\Delta H_M$, of nitrendipine crystals were analyzed by differential scanning calorimetry (Perkin Elmer DSC 7, USA). Two-point calibration using indium and tin was carried out to check the temperature axis and heat flow of the equipment. Starting material of 3–4 milligram was accurately weighed into standard aluminium pans and analyzed at a scanning rate of 10°C/min from 30°C to 230°C. This was done in a dry nitrogen atmosphere at flow rate 40 ml/min, and an empty aluminium pan was used as a reference.

## RESULTS

### Nitrendipine Crystalline Solubility and Amorphous Solubility Advantage

The HPLC method for determination of nitrendipine solubility was well validated. The standard curve linearity was verified from 0.05 to 20 μg/ml with an $r^2$ value of at least 0.999. The inter- and intra-day variability of low, medium and high concentrations was less than 2% RSD. The solubility of nitrendipine was 0.83±0.07 μg/ml in pure water at 2°C. The organic solvent demonstrated a certain cosolvent capacity, and the solubility was about 1.50±0.12 μg/ml when the cosolvent volume fraction was 0.09 (ratio of organic solvent to aqueous phase was 0.1, and no PVA in the system). This ratio was adopted in subsequent experiments to obtain a high degree of supersaturation and crystal yield.

The solubility of crystalline nitrendipine in the crystallization medium containing 0.25% PVA, Poloxamer 407 and HPMC was also determined and above the value without polymers of 1.50±0.12 μg/ml (Fig. 1a). The increase of solubility indicated that the polymers have an effect on the activity coefficient of drug molecules due to the intermolecular interactions between nitrendipine and polymers (34). Nitrendipine had a lower solubility in 0.25% Poloxamer 407 than that in 0.25% PVA and HPMC. This might be because 0.25% Poloxamer 407 had weaker intermolecular interactions with nitrendipine than that of 0.25% PVA and HPMC. Poloxamer 407 is a surfactant and has a great solubilizing effect when the concentration was above its critical micellization concentration (CMC) value. However, 0.25% of concentration was below its CMC, which was reported to be 0.7% at 25°C, and lower temperature also resulted in higher CMC values (35). Thus, no significant solubilizing effect was observed using 0.25% Poloxamer 407. Figure 1b shows the solubility of crystalline nitrendipine in crystallization medium at different temperatures. The crystalline solubility increased with the temperature. Thus, higher supersaturation can be obtained at 2°C than that at 15°C and 35°C.

As obtained from DSC, the melting peak and $\Delta H_M$ of nitrendipine is 157.8°C and 37.85±1.12 kJ/mol, respectively. Using Eq. 1, the theoretical estimated amorphous solubility advantage of nitrendipine is 403 times higher than that of crystalline state. Although the amorphous solubility obtained using this method is only true in theory, and the experimental amorphous solubility often reaches only a fraction of the theoretical value and is usually affected by the solvent and the polymers (34,36–38). The solubility advantage of amorphous phase with respect to crystalline phase provides an indication of the theoretical driving force for the nucleation and growth of crystalline phase.

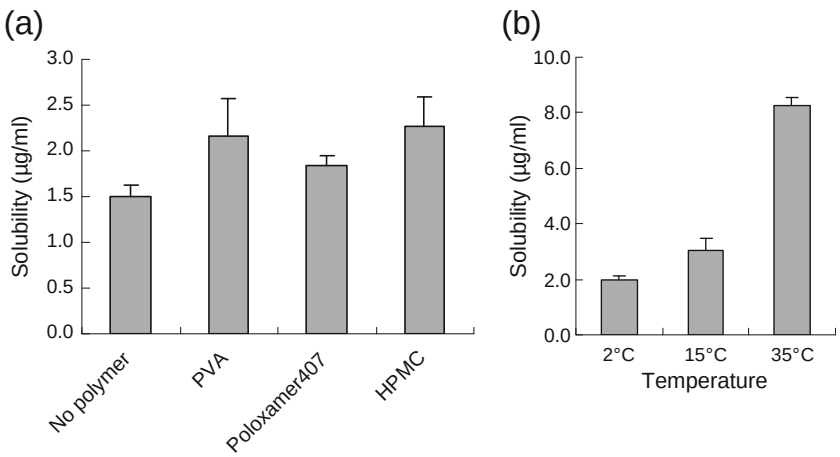


**Fig. 1** Nitrendipine crystalline solubility in crystallization medium containing different polymers (**a**), and at different temperatures (**b**) ($n=3$).

## Viscosity of Crystallization Medium and Diffusion Coefficient

The viscosity of the crystallization medium containing 0.25% PVA, HPMC and Poloxamer 407 and the effect of temperature on the viscosity of crystallization medium containing PVA were investigated using U-tube Viscometer. The results are shown in Fig. 2. Poloxamer 407 has the lowest viscosity compared with PVA and HPMC (Fig. 2a). The dynamic viscosity of the crystallization medium was decreased with increasing temperature (Fig. 2b).

In the case of the diffusion-controlled growth mechanism, the crystal growth rate and final particle size can be influenced by the diffusion of the solute. The relationship between the diffusion coefficient, $D$, viscosity, $\eta$, and temperature, $T$, can be expressed by the Stokes-Einstein relationship (39):

$$D = \frac{kT}{3\pi\eta r} \tag{5}$$

where $r$ is the molecular diameter. Decreasing the temperature and increasing the viscosity can result in a decrease in the diffusion coefficient.

## Effect of Different Process Parameters on the Size and Shape of Nitrendipine Crystals

### *Effect of PVA, HPMC and Poloxamer 407*

In order to find appropriate growth conditions for nitrendipine spherical crystals, different parameters were investigated by comparing their initial particle size, final crystal size and shape. The typical shape of final nitrendipine crystals is presented in Fig. 3.

Three kinds of polymers, i.e. HPMC, Poloxamer 407 and PVA, with a concentration of 0.25% (m/v) were introduced into the aqueous phase. The mixing of drug organic solution with the aqueous solution containing PVA resulted in a milky suspension. When the suspension was diluted three times, a semi-transparent suspension with a blue opalescence was obtained, which indicated presence of particles in nanometer size range. The initial particle size was determined and indicated that the smallest initial particle size ($0.15 \pm 0.02$ μm) with the narrowest particle size distribution (Span $= 0.36 \pm 0.01$) was observed using PVA. Prolonged incubation at 2°C for five hours resulted in the formation of precipitate that collected at the bottom of the vials. Optical microscopy revealed that spherical crystals with a smooth surface and uniform particle size were obtained (Fig. 3a). When Poloxamer 407 was present in the aqueous phase, the initial particle size is $2.69 \pm 0.92$ μm with a wide particle size distribution (span $= 17.71 \pm 2.35$). The crystals had a needle and star-like shape (Fig. 3b). In the case of HPMC, initial particle size is $0.34 \pm 0.17$ μm and span is $1.66 \pm 0.41$. Spherical crystals with a rough surface were obtained (Fig. 3c). PVA showed good crystal growth inhibition ability and was used as stabilizer in all subsequent experiments.

### *Effect of Temperature*

The temperature also influences the initial particle size and shape of final crystals. When the temperature increased from 2°C to 35°C, the initial particle size increased markedly from $0.15 \pm 0.02$ μm to $17.01 \pm 4.13$ μm, and the crystal shape changed from monodispersed spherical crystals to needle or star-like crystals (Fig. 3a, d, e). From the results of this study, the optimal temperature for anti-solvent precipitation was found to be approximately 2°C, and, accordingly, all subsequent experiments were conducted at 2°C.

### *Effect of PEG 200 Content in the Organic Phase*

The effect of the PEG 200 content in the organic phase was investigated when the drug concentration, PVA concentration and temperature were fixed at 30 mg/ml, 0.5% and 2°C, respectively. The initial particle size decreased from $0.18 \pm 0.02$ μm to $0.13 \pm 0.02$ μm, as the PEG 200 content in the organic phase increased from 0% to 100% ($P < 0.05$). The crystal growth rate was retarded by the presence of PEG 200, and the final crystal size was reduced as the PEG 200 content increased (Fig. 4a). The presence of PEG 200 also modified the crystal shape. As shown in Fig. 3f (arrow

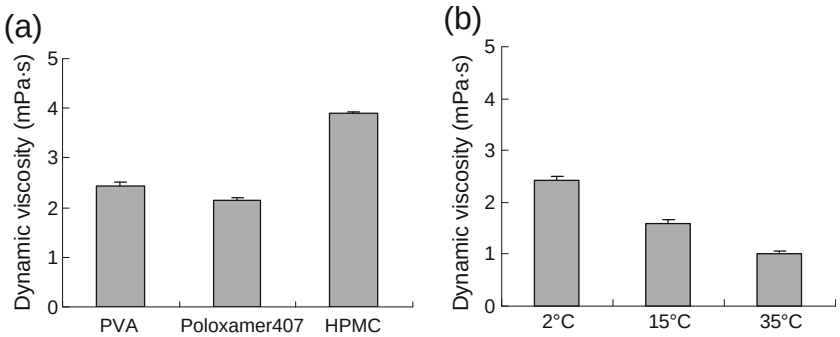


**Fig. 2** Dynamic viscosity of crystallization medium containing different polymers (**a**), and at different temperatures (**b**) ($n = 3$).

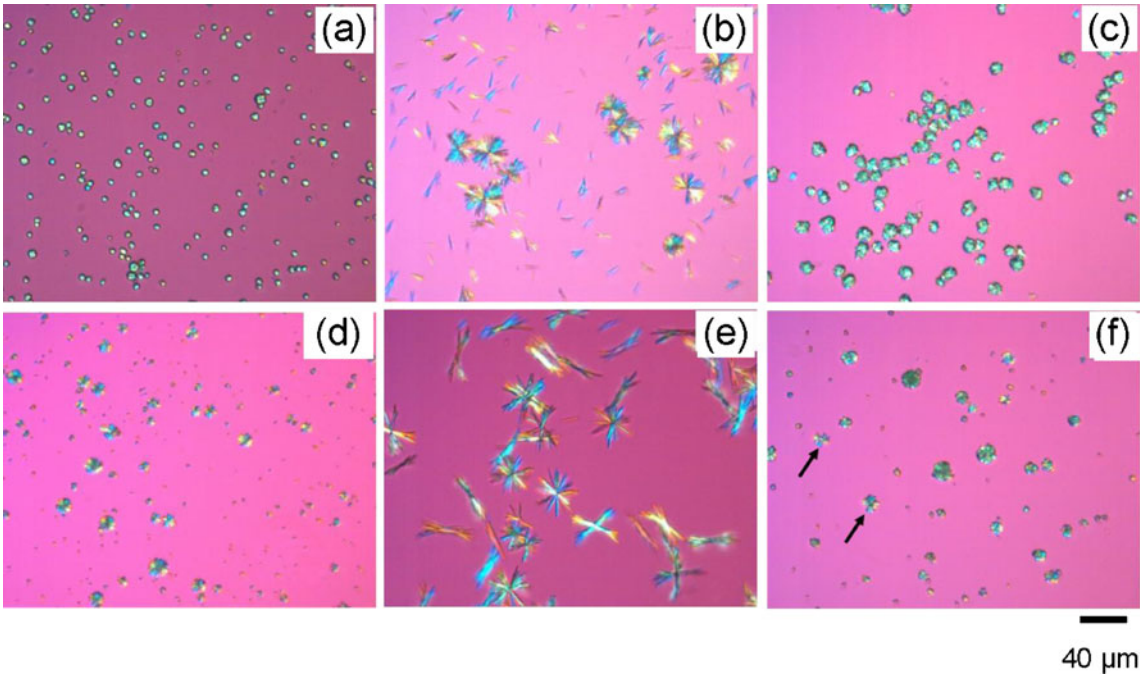


**Fig. 3** Optical microscopy evaluation of morphology of final crystals obtained with different conditions. Different kinds of polymers (other conditions: 2°C, 30 mg/ml drug, 50% PEG 200 in organic phase): PVA (**a**), Poloxamer 407 (**b**), HPMC (**c**). Dfferent temperatures (other conditions: 30 mg/ml drug, 0.25% PVA, 50% PEG 200): 15°C (**d**), 35°C (**e**); no PEG 200 present in organic phase (**f**).

indicated), some star-like crystals with a wider particle size distribution could be observed in the absence of PEG 200. In subsequent experiments, the PEG 200 content in the organic phase was 50%.

### *Effect of PVA Concentration in the Aqueous Phase*

The initial particle size decreased as the PVA concentration increased. At the lowest PVA concentration (0.1%), the initial particle size was 0.30±0.07 μm, while a plateau was reached where the particle size and size distribution were approximately 0.14 μm and 0.36, respectively, and hardly changed with increasing PVA concentrations from 0.5% to 2.0%. The final particle size, as shown in Fig. 4b, decreased with increasing PVA concentrations.

### *Effect of Drug Concentration in the Organic Phase*

The effect of the drug concentration was investigated when the PVA concentration was fixed at 0.15%. The initial

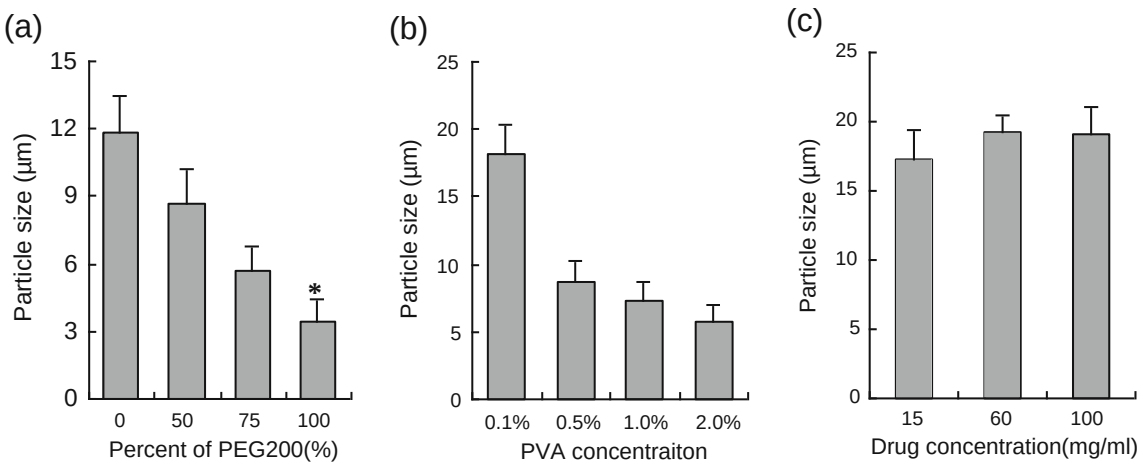


**Fig. 4** Particle size of spherical crystals obtained at different conditions. Effects of PEG 200 content (**a**), PVA concentration (**b**) and drug concentration (**c**) on the final crystal size ($n = 3$). *Drug concentration was 15 mg/ml due to the limited saturation solubility of nitrendipine in pure PEG 200.

particle size increased from 0.14±0.01 μm to 2.11± 0.87 μm, and size distribution from 0.36±0.01 to 20.73± 2.13 as the drug concentration in the organic phase increased from 15 mg/ml to 100 mg/ml. This is most likely the result of significant agglomeration from the very early stage of the experiments. It seems that the particle size of the final crystals is independent of the drug concentration, and no significant difference in the final crystal size was observed at different drug concentrations in the organic phase ($P$=0.34) (Fig. 4c).

## DISCUSSION

The newly precipitated particles had a diameter of about 0.14 μm, and the particles grew to the micrometer range in five hours after the precipitation. As illustrated in Fig. 5a, the morphology of the final crystals showed a spherical shape with a narrow particle size distribution. When these spherical particles were viewed under a transmitted polarized optical microscopy, the characteristic Maltese-cross pattern was observed (Fig. 5b), which has the similar feature of polymer spherulites (40). From the surface topography, it appears that spherical crystals were formed by the aggregation of nanoparticles (Fig. 5d), but the XRPD (Fig. 6b) proved that the spherical particles had a crystalline structure, and the crystalline form is the same as that of starting material (Fig. 6c). However, the lower intensity of spherical crystals might be due to the lower crystallinity of the samples. The crystalline form is RS-mode.I, which demonstrated identical XRPD patterns as that published in CCDC (reference code JEXKUS) (41,42).

These monodispersed spherical crystals can only be formed in the systems containing PVA and PEG 200 in lower temperature (2°C). How did those colloidal nanoparticles grow as monodispersed spherical crystals? To investigate the growth mechanism of nitrendipine spherical crystals, the precipitated solid material was collected by passing the solution through a membrane filter (0.1 μm, Membrane-solutions, Shanghai, China) at different time intervals and then blow-drying at room temperature. A series of SEM images were recorded and illustrated in Fig. 7.

### Formation and Aggregation of Amorphous Nanoparticles

At the early stage of precipitation, as illustrated in Fig. 7a, nitrendipine molecules clustered together to form spherical nanoparticles. The low solubility of nitrendipine in the aqueous phase is important to achieve a sufficient initial supersaturation, which is needed to produce a sufficient number of nanoparticles. Without the stabilization of PVA, these nanoparticles agglomerated instantly due to their hydrophobic surface to form a sticky rubbery state material. XRPD proved that this rubbery state material is predominantly amorphous form (Fig. 6a). A particular feature of polymer-mediated precipitation is the potential for oriented aggregation of primary particles (29). If crystallization takes place *via* a multistep growth mechanism, a complex crystal morphology can be produced. In this case, the polymer additives interact with primary nanoparticles and have marked effects on the very early stages of crystal growth. Temporary stabilization of these primary units by interaction with the polymers

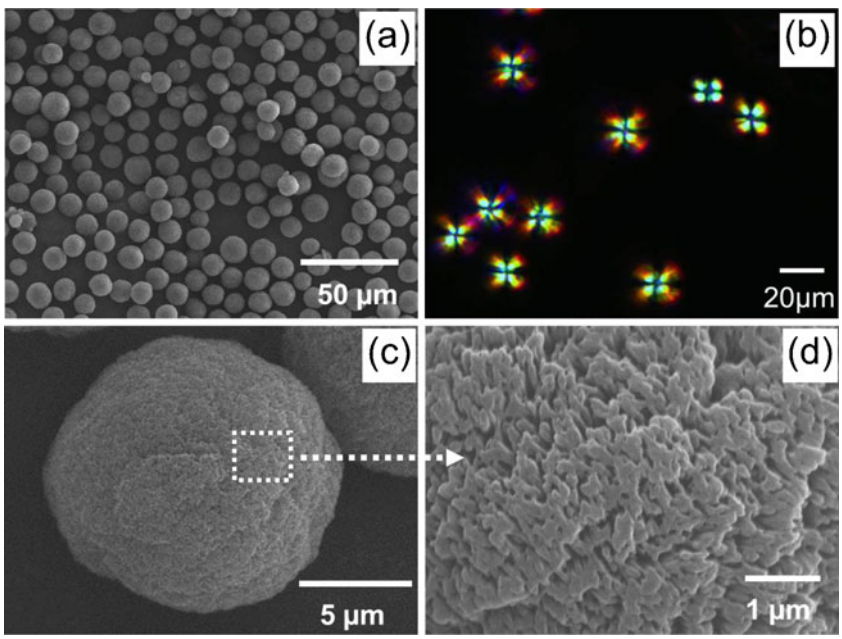


**Fig. 5** SEM and polarized optical microscopy images of the nitrendipine spherical crystals. (**a**) Low magnification sphere morphology of the crystals; (**b**) observed by polarized optical microscopy; (**c**) enlarged single spherical crystals; (**d**) high magnification image of a spherical crystal marked with a rectangle in (**c**), revealing the detailed structure of the surface. (Precipitation conditions: 0.25% PVA; 50% PEG 200 in organic phase; 80 mg/ml drug in organic phase; precipitation temperature: 2°C).

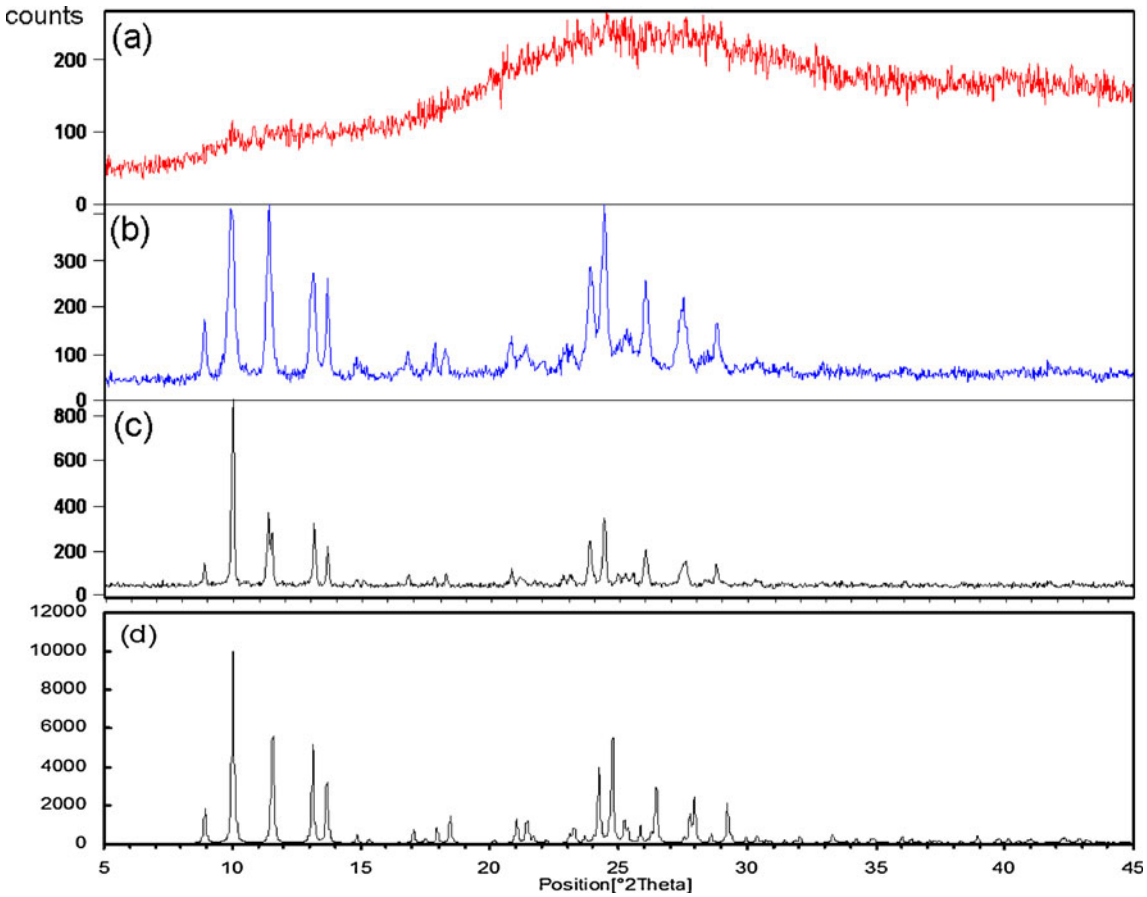


**Fig. 6** XRPD patterns of the samples. (**a**) Amorphous agglomerates; (**b**) spherical crystals; (**c**) nitrendipine starting material; (**d**) XRPD patterns of nitrendipine published in CCDC (Reference code: JEXKUS).

retards further growth in a molecular fashion, such that aggregation of these nanoparticles proceeds more rapidly than the growth of individual particles, resulting in the formation of aggregates. This aggregation process was confirmed by Fig. 7b, as the arrow indicated.

## Ripening of Amorphous Nanoparticles into Star-Like Templates Through Dissolution-Recrystallization Pathway

Crystallization often proceeds by a sequential process rather than a single-step pathway (24). The precursor nanoparticles obtained by the precipitation of nitrendipine in the aqueous phase are amorphous and, subsequently, are transformed into a crystalline form. The Ostwald rule of stages states that an unstable system is not necessarily transformed directly into the most stable state, but into another transient state whose formation from the original is accompanied by the smallest loss of free energy (43). In this process, the amorphous particles are first formed because their lower interfacial free energy results in a lower nucleation energy barrier compared to the crystalline form. Nevertheless, the subsequent formation of the crystalline phase indicates that the amorphous phase is metastable with respect to the crystalline phase (44,45). This process is similar to the diffusion-controlled Ostwald ripening (46,47). This ripening process takes place because there is an excess solubility in the solvent of the dispersed phase. For such an anti-solvent precipitation system, the solubility of amorphous particles was greatly higher than that of the crystalline form. The solubility difference between amorphous and crystalline makes the bulk supersaturated with respect to the crystalline. Thus, the amorphous particles tend to be transformed into a crystalline form. Once the crystalline phase is formed, it will grow rapidly with the amorphous nanoparticles acting as a reservoir. This process takes place through the dissolution of the amorphous nanoparticles and is followed by recrystallization on the surface of the formed aggregates. For that, the crystalline phase is most likely arranged in a radial fashion around a core, and subsequent growth of the radial structure is markedly affected by the core. This step could be a diffusion rate-controlled process. Thus, the polymers have a marked effect on the crystal growth

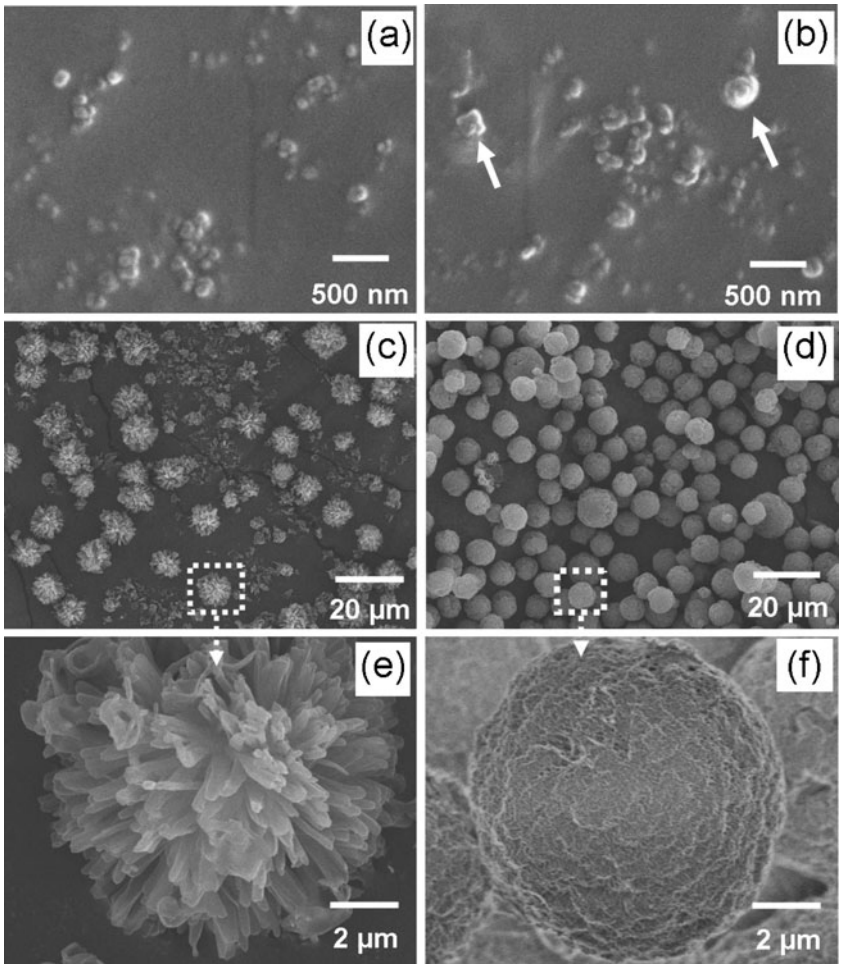


**Fig. 7** SEM images of the precipitated particles sampled at different time intervals after mixing of aqueous phase and organic phase. (**a**) 0 min; (**b**) 10 min; (**c**) 40 min; (**d**) 1.5 h; (**e**) high magnification image of a star-like crystal (marked with a rectangle in (**c**)); (**f**) high magnification image of a spherical crystal (Precipitation conditions: 0.25% PVA; 50% PEG 200 in organic phase; 30 mg/ml drug in organic phase; precipitation temperature: 2°C)

rate. Increasing the viscosity and adsorption of polymers on the surface of growing crystals could slow down the transformation process.

Forty minutes after the precipitation, some star-like particles were formed, as indicated in Fig. 7c. Examination of particles at a high magnification strongly suggested that the particles were constructed from small needle-like distinct crystalline units arranged radially around a center (Fig. 7e), and these star-like particles served as templates for the formation of spherical crystals. How did those needle-like crystalline units form? According to the surface energy theory, the equilibrium shape of a crystal is related to the free energy of the faces; in other words, the crystal faces would grow at a rate proportional to their respective energy (26,48). The side faces show a large nucleation barrier for growth, whereas the top faces possess a much smaller barrier, so the side faces grow much more slowly than the top faces (49). At these high degrees of supersaturation, all the top faces grow extremely rapidly, whereas the side faces still grow relatively slowly, resulting in a needle-like morphology (50). When we consider a single needle of these units, as if it were a tip with a local diffusion field around it (Fig. 9f), the following expression can be written for the growth rate of the needle (51):

$$v_{needle} = \frac{4kDV_{mol}(C_b - C_s)}{R} \tag{6}$$

where $v_{needle}$ is the growth rate of the needle, $C_b$ is the bulk concentration of solute, $C_s$ is the surface concentration of solute, $k$ is a geometric correction factor, $D$ is the diffusion constant, and $V_{mol}$ is the volume of one molecule, and $R$ is the radius of the needle tip. From the above equation, we can easily conclude that the increase in viscosity of the solution and the decrease in temperature lead to a decrease in the diffusion constant, resulting in a slower needle growth rate.

## Filling the Gap Between the Needle-Like Distinct Crystalline Units

Prolonged incubation of the sample for one and a half hours resulted in the formation of a precipitate that collected at the bottom of the vials, suggesting that the crystal growth had reached equilibrium. SEM observa-

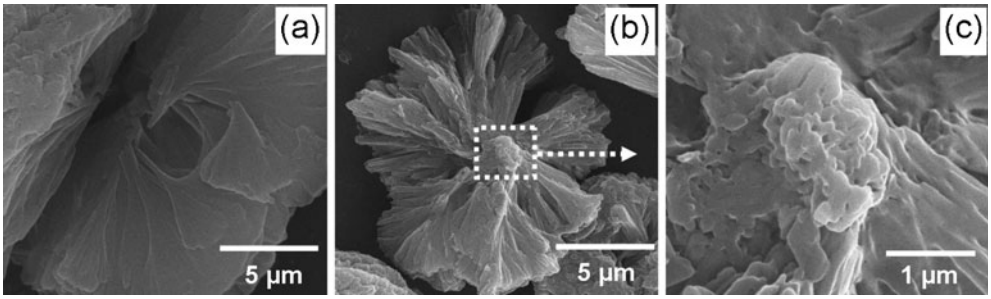


**Fig. 8** (**a** and **b**) Radiating spherical pattern in the interior of a cracked open spherical crystal. (**c**) High magnification image of a core (marked with a rectangle in (**b**)) shows assembly of nanoparticle building units.

tion of the crystals (Fig. 7d and f) indicated that the crystals had a spherical shape with a uniform particle size. Compared with Fig. 7c, the gap between the needles was filled. This process is just like the model of contact recrystallization (47,52). As illustrated in Fig. 9g, the driving force of this process, ($\Delta\mu$), can be written as

$$\Delta\mu = RT\ln\frac{C_1}{C_2} = \gamma V_m\left[\frac{2}{r_1} - \left(\frac{1}{r_{2a}} + \frac{1}{r_{2b}}\right)\right] \quad (7)$$

where $C_1$ and $C_2$ are the concentrations of nitrendipine in equilibrium with the radii $r_1$ and $r_2$, respectively, $r_1$ is the radius of the needle tip, $r_{2a}$ is the longitudinal negative radius of the curvature in the boundary region of two needle units in contact, and $r_{2b}$ is the latitudinal positive radius, $\gamma$ is the liquid-solid surface tension and $V_m$ is the solid molar volume. When the gap between needles was reduced to a certain width, the absolute value of $r_{2a}$ is very small. In this case, we believe that most needles cease to grow longitudinally. The nitrendipine molecules are deposited preferentially in the confined space compared with the needle tip, owing to the negative radius of curvature ($r_{2a}$), resulting in the filling of the gap between needles by consuming the rest of the amorphous particles until the system approaches equilibrium at the end of the experiment.

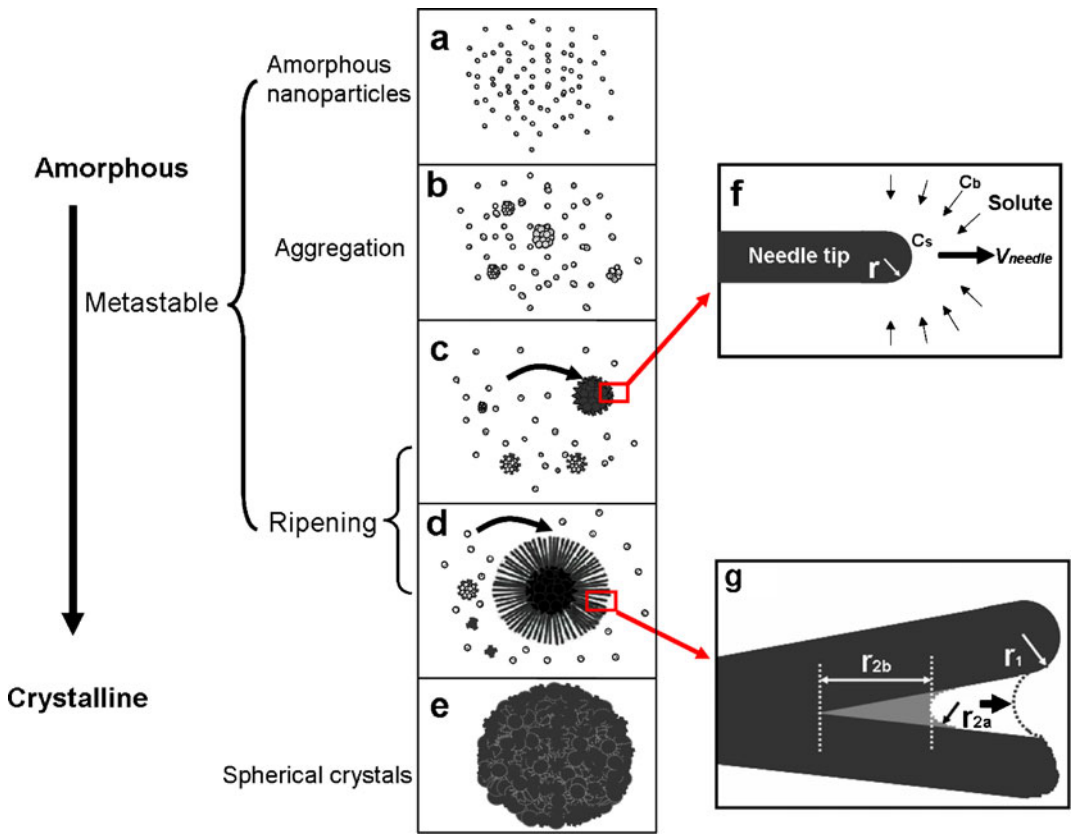


**Fig. 9** Schematic illustration of the formation mechanism of nitrendipine spherical crystals. (**a**) Formation of amorphous nanoparticles; (**b**) agglomeration to generate a core for the formation of a star-like template; (**c** and **d**) formation of star-like templates though ripening; (**e**) spherical crystals formed by filing the gap between the needle-like distinct crystalline units; (**f**) model for the growth of needle-like distinct crystalline units; (**g**) model for the filling of the gap between needle-like distinct crystalline units.

To further explore how such a superstructure was formed, the sample was crushed. The cracked nitrendipine spherical crystals are shown in Fig. 8a and b, and it can be seen that they have a characteristic radiating feature. We believe that there may be a core which controls the construction of the spherical superstructure, and the outer radial structure grows with a radial alignment pointing to the inner core center. High magnification SEM observation of the fractured core is shown in Fig. 8c. It can be inferred that the core was formed through the assembly of nanoparticle building units, although many nanoparticles in the core were fused together during growth process, which also confirmed that aggregation took place at the beginning of the crystal growth.

Why were these spherical crystals only formed at a lower temperature? It can be inferred that the aggregation of primary nanoparticles played an important role in the formation of spherical crystals. At the early stage of crystal growth, the aggregation of the resulting primary nuclei and diffusional growth of individual nuclei via molecule-by-molecule addition are two competing mechanisms of the crystal growth mechanism. At a lower temperature, crystallization can proceed much easier along the aggregation pathway when there are large number of nanoparticles, and the solubility is low (53). However, at a higher temperature, the solubility is sufficiently high, resulting in lower supersaturation, giving rise to fewer primary nanoparticles. In addition, the increased molecular diffusion rate and reaction kinetics at the crystal boundary layer interface make classical crystallization via a molecule-by-molecule addition the dominant crystallization mechanism, and resulting in a fast transformation speed of amorphous nanoparticles to crystalline phase. Thus, the nanoparticle aggregates which are necessary for the formation of star-like templates with sufficient needlelike subunits for spherical crystals cannot be formed at a higher temperature.

From the above results, a growth model can be formulated to account for the formation mechanism of the monodispersed spherical crystals in the presence of polymer additives, as summarized in Fig. 9. Spherical micro-crystals were formed by the following steps: (1) precipitation of amorphous nanoparticles; (2) aggregation of amorphous nanoparticles to form a core; (3) ripening of amorphous nanoparticles into star-like templates; (4) formation of spherical crystals by filling the gap between the needle-like distinct crystalline units with dissolved molecules from the remaining amorphous phase.

## CONCLUSIONS

In the anti-solvent crystallization system, the morphology of nitrendipine crystals was affected by the polymers, the temperature, and the presence of PEG 200. Monodispersed micro-spherical crystals were obtained when PVA and PEG 200 were present in the precipitation system and the temperature was 2°C. The particle size of nitrendipine spherical crystals was affected by the PVA concentration in the aqueous phase and the PEG 200 content in organic phase.

The growth of monodispersed spherical crystals involved the following steps: First nitrendipine precipitated as large number of amorphous nanoparticles when a nitrendipine organic solution was introduced into the aqueous phase. Second, the amorphous nanoparticles aggregated to form a core, accompanied by transformation into a crystalline form. Once the crystalline form was obtained, it grew rapidly on the surface of the aggregates. During this process, the amorphous particles were acting as a reservoir to form star-like particles. These star-like particles were constructed from small needle-like distinct crystalline units arranged radially around a center and served as templates for the formation of spherical crystals. Finally, the gap between the needle-like distinct crystalline units was filled by consuming the remaining amorphous particles to form a single spherical crystal. These findings provide a new insight into spherulitic crystallization of pharmaceutical ingredient and have important implications for the understanding of anti-solvent crystallization.

## ACKNOWLEDGMENTS & DISCLOSURES

We are grateful for financial support from the National Natural Science Foundation (No. 30873182) and National Basic Research Program of China (973 Program) (No. 2009CB930302). The grant from Lundbeckfonden (Copenhagen, Denmark) for the purchase of X-ray power diffractometer is also acknowledged (grant decision 479/06).

## REFERENCES

1. Erdemir D, Lee AY, Myerson AS. Nucleation of crystals from solution: classical and two-step models. Acc Chem Res. 2009;42:621–9.
2. Garcia E, Veesler S, Boistelle R, Hoff C. Crystallization and dissolution of pharmaceutical compounds: an experimental approach. J Cryst Growth. 1999;198–199:1360–4.
3. Blagden N, de Matas M, Gavan PT, York P. Crystal engineering of active pharmaceutical ingredients to improve solubility and dissolution rates. Adv Drug Deliv Rev. 2007;59:617–30.
4. Watanabe A, Yamaoka Y, Takada K. Crystal habits and dissolution behaviours of aspirin. Chem Pharm Bull. 1982;30:2958–63.
5. Xia D, Cui F, Piao H, Cun D, Jiang Y, Ouyang M, *et al.* Effect of crystal size on the *in vitro* dissolution and oral absorption of nitrendipine in rats. Pharm Res. 2010;27:1965–76.
6. Li X, Wang J, Shen Z, Zhang P, Chen J, Yun J. Preparation of uniform prednisolone microcrystals by a controlled microprecipitation method. Int J Pharm. 2007;342:26–32.

7. Matteucci ME, Paguio JC, Miller MA, Williams 3rd RO, Johnston KP. Highly supersaturated solutions from dissolution of amorphous itraconazole microparticles at pH 6.8. Mol Pharm. 2009;6:375–85.
8. Douroumis D, Fahr A. Stable carbamazepine colloidal systems using the cosolvent technique. Eur J Pharm Sci. 2007;30:367–74.
9. Lindfors L, Forssén S, Westergren J, Olsson U. Nucleation and crystal growth in supersaturated solutions of a model drug. J Colloid Interface Sci. 2008;325:404–13.
10. Wen H, Morris KR, Park K. Hydrogen bonding interactions between adsorbed polymer molecules and crystal surface of acetaminophen. J Colloid Interface Sci. 2005;290:325–35.
11. Wei H, Shen Q, Zhao Y, Wang D, Xu D. Influence of polyvinylpyrrolidone on the precipitation of calcium carbonate and on the transformation of vaterite to calcite. J Cryst Growth. 2003;250:516–24.
12. Berkovitch-Yellin Z. Toward an ab initio derivation of crystal morphology. J Am Chem Soc. 1985;107:8239–53.
13. Piana S, Reyhani M, Gale JD. Simulating micrometre-scale crystal growth from solution. Nature. 2005;438:70–3.
14. Andreassen JP. Formation mechanism and morphology in precipitation of vaterite-nano-aggregation or crystal growth? J Cryst Growth. 2005;274:256–64.
15. Shen Q, Wei H, Wang L, Zhou Y, Zhao Y, Zhang Z, *et al.* Crystallization and aggregation behaviors of calcium carbonate in the presence of poly(vinylpyrrolidone) and sodium dodecyl sulfate. J Phys Chem B. 2005;109:18342–7.
16. Sugimoto T, Dirige GE, Muramatsu A. Formation mechanism of monodisperse CdS particles from concentrated solutions of Cd-EDTA complexes. J Colloid Interface Sci. 1996;182:444–56.
17. Liu Z, Wen XD, Wu XL, Gao YJ, Chen HT, Zhu J, *et al.* Intrinsic dipole-field-driven mesoscale crystallization of core-shell ZnO mesocrystal microspheres. J Am Ceram Soc. 2009;131:9405–12.
18. Magill JH. Spherulites: a personal perspective. J Mater Sci. 2001;36:3143–64.
19. Krebs MRH, MacPhee CE, Miller AF, Dunlop IE, Dobson CM, Donald AM. The formation of spherulites by amyloid fibrils of bovine insulin. PNAS. 2004;101:14420–4.
20. Reiss H. The growth of uniform colloidal dispersions. J Chem Phys. 1951;19:482–7.
21. LaMer VK, Dinegar RH. Theory, production and mechanism of formation of monodispersed hydrosols. J Am Chem Soc. 1950;72:4847–54.
22. Privman V, Goia DV, Park J, Matijevic E. Mechanism of formation of monodispersed colloids by aggregation of nanosize precursors. J Colloid Interface Sci. 1999;213:36–45.
23. Park J, Privman V, Matijevic E. Model of formation of monodispersed colloids. J Phys Chem B. 2001;105:11630–5.
24. Cölfen H, Mann S. Higher-order organization by mesoscale self-assembly and transformation of hybrid nanostructures. Angew Chem Int Ed. 2003;42:2350–65.
25. Haberkorn H, Franke D, Frechen T, Goesele W, Rieger J. Early stages of particle formation in precipitation reactions-quinacridone and boehmite as generic examples. J Colloid Interface Sci. 2003;259:112–26.
26. Mullin JW (ed). Crystallization (4th Ed.), Butterworth-Heimemann, Oxford: 2001.
27. Penn RL. Kinetics of oriented aggregation. J Phys Chem B. 2004;108:12707–12.
28. Penn RL, Oskam G, Strathmann TJ, Searson PC, Stone AT, Veblen DR. Epitaxial assembly in aged colloids. J Phys Chem B. 2001;105:2177–82.
29. Kulak AN, Iddon P, Li Y, Armes SP, Cölfen H, Paris O, *et al.* Continuous structural evolution of calcium carbonate particles: a unifying model of copolymer-mediated crystallization. J Am Chem Soc. 2007;129:3729–36.
30. Gránásy L, Pusztai T, Tegze G, Warren JA, Douglas JF. Growth and form of spherulites. Phys Rev E. 2005;72:1–15.
31. Hutter JL, Bechhoefer J. Banded spherulitic growth in a liquid crystal. J Cryst Growth. 2000;217:332–43.
32. Lindfors L, Forssn S, Skantze P, Skantze U, Zackrisson A, Olsson U. Amorphous drug nanosuspensions. 2. experimental determination of bulk monomer concentrations. Langmuir. 2006;22:911–6.
33. Brick MC, Palmer HJ, Whitesides TH. Formation of colloidal dispersions of organic materials in aqueous media by solvent shifting. Langmuir. 2003;19:6367–80.
34. Matteucci ME, Brettmann BK, Rogers TL, Elder EJ, Williams RO, Johnston KP. Design of potent amorphous drug nanoparticles for rapid generation of highly supersaturated media. Mol Pharm. 2007;4:782–93.
35. Alexandridis P, Holzwarth JF, Hatton TA. Micellization of poly (ethylene oxide)-poly(propylene oxide)-poly(ethylene oxide) triblock copolymers in aqueous solutions: thermodynamics of copolymer association. Macromolecules. 1994;27:2414–25.
36. Alonzo D, Zhang G, Zhou D, Gao Y, Taylor L. Understanding the behavior of amorphous pharmaceutical systems during dissolution. Pharm Res. 2010;27:608–18.
37. Hancock BC, Parks M. What is the true solubility advantage for amorphous pharmaceuticals? Pharm Res. 2000;17:397–404.
38. Matteucci ME, Miller MA, Williams RO, Johnston KP. Highly supersaturated solutions of amorphous drugs approaching predictions from configurational thermodynamic properties. J Phys Chem B. 2008;112:16675–81.
39. Jackson KA (ed.). Kinetic processes: crystal growth, diffusion, and phase transitions in materials, WILEY-VCH Verlag GmbH & Co. KGaA, Weinheim: 2004.
40. Bower DI (ed.). an introduction to polymer physics. Cambridge University Press, Cambridge, New York: 2002.
41. Burger A, Rollinger JM, Brüggeller P. Binary system of (R)- and (S)-nitrendipine—polymorphism and structure. J Pharm Sci. 1997;86:674–9.
42. Langs DA, Strong PD, Triggle DJ. Receptor model for the molecular basis of tissue selectivity of 1,4-dihydropyridine calcium channel drugs. J Comput Aided Mol Des. 1990;4:215–30.
43. Threlfall T. Structural and thermodynamic explanations of Ostwald's Rule. Org Process Res Dev. 2003;7:1017–27.
44. Zhang TH, Liu XY. How does a transient amorphous precursor template crystallization. J Am Chem Soc. 2007;129:13520–6.
45. Lindfors L, Skantze P, Skantze U, Westergren J, Olsson U. Amorphous drug nanosuspensions. 3. particle dissolution and crystal growth. Langmuir. 2007;23:9866–74.
46. Lindfors L, Skantze P, Skantze U, Rasmusson M, Zackrisson A, Olsson U. Amorphous drug nanosuspensions. 1. inhibition of ostwald ripening. Langmuir. 2006;22:906–10.
47. Sugimoto T (ed.). Monodispersed particles, Elsevier Science B.V., Amsterdam-London-New York-Oxford-Paris-Shannon-Tokyo: 2001.
48. Boerrigter SXM, Hollander FFA, van de Streek, Bennema P, Meekes H. Explanation for the needle morphology of crystals applied to a β′ Triacylglycerol. Cryst Growth Des. 2002;2:51–4.
49. Cuppen HM, Beurskens G, Kozuka S, Tsukamoto K, Smits JMM, de Gelder R, *et al.* Crystal structure and growth behavior of aspartame form I-A. Cryst Growth Des. 2005;5:917–23.
50. Cuppen HM, van Eerd ART, Meekes H. Needlelike morphology of aspartame. Cryst Growth Des. 2004;4:989–97.
51. Heijna MCR, Theelen MJ, van Enckevort WJP, Vlieg E. Spherulitic growth of hen egg-white lysozyme crystals. J Phys Chem B. 2007;111:1567–73.
52. Sugimoto T, Yamaguchi G. Contact recrystallization of silver halide microcrystals in solution. J Cryst Growth. 1976;34:253–62.
53. Ma Y, Cölfen H, Antonietti M. Morphosynthesis of Alanine mesocrystals by pH control. J Phys Chem B. 2006;110:10822–8.